This article has been accepted for publication in a future issue of this journal, but has not been fully edited. Content may change prior to final publication. Citation information: DOI 10.1109/JSTARS.2020.3003480, IEEE Journal of Selected Topics in Applied Earth Observations and Remote Sensing

Quantitative Analysis of Aerosol Influence on Suomi-NPP VIIRS Nighttime Light in China

Xuejun Wang, Xihan Mu, and Guangjian Yan, *Member, IEEE*

***Abstract*—as a primary nighttime light (NTL) data source, the Day/Night Band (DNB) sensor of the Visible Infrared Imaging Radiometer Suite (VIIRS) is used in a wide range of studies. However, this signal is influenced by the atmosphere and may cause uncertainty while monitoring ground NTL. Given the lack of quantitative analysis of atmospheric effect on NTL, this study analyzes the relationship between VIIRS DNB NTL radiance and aerosol optical depth (AOD) in the urban areas of Beijing and three other Chinese cities of different urbanization levels. Results suggest a significantly negative relationship between NTL radiance and AOD. Linear and log-linear models generate similar coefficients of determination (R^2) for AOD and NTL data, which vary for different urban centers. In Beijing, where Aerosol Robotic Network (AERONET) observations are available, R^2 reached 0.655 between monthly NTL radiance and AOD. A slight decrease of R^2 occurred while using the Himawari AOD. The relationship between NTL radiance and AOD varies among cities. NTL radiance may decrease by approximately 10 $nW \cdot cm^{-2} sr^{-1}$ when daily AOD increases one unit. For Beijing, this decrease may be above 15 $nW \cdot cm^{-2} sr^{-1}$, which is comparable to the threshold used to extract urban areas. These findings underscore the importance of AOD in the application of NTL data that are potentially useful in the reconstruction of stable time series VIIRS DNB images by removing the aerosol effects.**

***Index Terms*—nighttime light, aerosol optical depth, NPP-VIIRS, atmospheric effect, quantitative analysis.**

I. Introduction

NIGHTTIME light (NTL) remote sensing data reflect the distribution and intensity of artificial light at night. The two main sources of NTL data are the Defense Meteorological Satellite Program–Operational Linescan System (DMSP OLS) and Visible Infrared Imaging Radiometer Suite (VIIRS) Day/Night Band (DNB) sensor, onboard the Suomi-National Polar-orbiting Partnership (S-NPP) and Joint Polar Satellite System (JPSS) satellite platforms [1]. DMSP OLS data were no longer the primary data being processed for NTL after 2013 when VIIRS DNB data were available. Compared with DMSP OLS, the VIIRS DNB has significant improvements on sensor resolution and calibration, which can acquire global daily nighttime visible and near-infrared (NIR) information from cities, towns, industrial sites, and other human activities [2]. These improvements allow for better monitoring of both the magnitude and signature of nighttime phenomena. The VIIRS DNB NTL images are used in a wide range of research fields: (1) demographic and socioeconomic indicators [3-9], (2) short-term features detection [10-13], (3) settlement dynamics [14-18], (4) nighttime atmospheric properties [19-25], (5) short- and long-term change detection [26-28], and (6) other topics, such as light pollution [29, 30] and CO_2 emissions [31, 32].

Numerous factors, including moonlight, atmosphere, snow, and clouds, affect the quality of NTL images [33] and adversely impact data application and analysis. Atmospheric scattering [34] and absorption [35] (especially atmosphere with high-concentration aerosols) can considerably affect the signal detected by the satellite sensor. Aerosol optical depth (AOD) is an important parameter in measuring the degree of atmospheric extinction that can also be used as an effective substitute to track the evolution of aerosol-induced air pollution [36]. The VIIRS DNB radiance is sensitive to changes of aerosols and thus can be used as an indicator of air quality changes [23]. Johnson *et al.* [19] and McHardy *et al.* [20] presented methods of retrieving nighttime AOD using the contrast between the adjacent VIIRS DNB pixels. Román *et al.* [37] proposed an atmospheric correction method for VIIRS DNB daily products. However, most studies and analyses do not consider aerosols when using NTL data. Limited research quantitatively explores the relationship between aerosols and NTL radiance.

Heavily polluted atmosphere with increased AOD may produce an even greater impact on the quality of NTL images. Air pollution is increasingly becoming severe in developing countries with the rapid economic growth and urbanization [38]. Air pollution in China gradually worsened since the year 2000 and has recently drawn public attention [39]. At present, air quality in China is improving due to adopted systematic measures[40, 41]. Therefore, analysis is important to determine the atmospheric effect and its extent on the NTL data in China.

This study aims to quantitatively investigate the relationship between NTL radiance and AOD using daily and monthly data in China. Four Chinese cities of different sizes and urbanization levels are selected as study areas. The urban centers are extracted and then two regression formulas are

Manuscript received; revised; accepted. This study was supported by the Foundation of the key program of National Natural Science Foundation of China (NSFC: Grant No.41331171). (*Corresponding author: Xihan Mu.*)

X. J. Wang, X. H. Mu and G. J. Yan are with the Beijing Engineering Research Center for Global Land Remote Sensing Products, Institute of Remote Sensing Science and Engineering, Faculty of Geographical Science, Beijing Normal University, Beijing 100875, China, and also with the State Key Laboratory of Remote Sensing Science, Jointly Sponsored by Beijing Normal University and Institute of Remote Sensing and Digital Earth of Chinese Academy of Sciences, Beijing 100875, China (e-mail: xuejunw@mail.bnu.edu.cn, muxihan@bnu.edu.cn and gjyan@bnu.edu.cn).

applied to evaluate the relationship between NTL radiance and AOD. The VIIRS DNB NTL data are adopted to study the quantitative impact of aerosols.

The paper is organized as follows. Section II introduces the study areas and data used. The data preprocess procedure, extraction of urban centers, statistical analysis, and linear regression are described in Section III. Results and discussion are found in Sections IV and V, respectively, and the conclusions are presented in Section VI.

II. Study Areas and Data

A. Study Areas

The four cities under study include Beijing in northern China, representing a highly urbanized and developed city. Chengdu in western China and Wuhan in central China are the respective capitals of Sichuan and Hubei provinces, representing large cities and regional economic centers. Meishan is a middle-sized city in Sichuan Province, representing cities undergoing urbanization (Fig. 1 and TABLE I).

Beijing (39.4°–41.6°N, 115.7°–117.4°E) is the capital of China and is located in the northern part of the North China Plain. This area is characterized by monsoon-influenced semi-humid continental climate and features a high-temperature rainy summer, cold and dry winter, and short spring and autumn. Beijing is one of the largest cities in the world and has become heavily polluted due to rapid urbanization and industrialization over the past two decades [38]. Systematic measures such as the desulfurization treatment in coal-fired power plants [42] and upgrading fuels for vehicles [43] have been applied. Thus, air pollution has been alleviated in recent years.

Wuhan (29°58′–31°22′N, 113°41′–115°05′E) is located in the eastern part of the Jianghan Plain and at the intersection of the Yangtze and Han Rivers. This area is a subtropical humid southeast monsoon climate zone with abundant rainfall and heat, cold winter and hot summer, and distinct four seasons. Chengdu (30°5′–31°26′N, 102°54′–104°53′E) is located in the western part of Sichuan Basin and the eastern edge of Qinghai–Tibet Plateau. The overall terrain is high in the northwest and low in the southeast. Chengdu is a subtropical humid and semi-humid monsoon climate zone with a mild climate, long frost-free period, abundant rainfall, and limited sunshine. Meishan (29°24′–30°16′N, 102°49′–104°30′E) is located in the southwestern part of the Chengdu Plain in the Sichuan Basin and the climate is similar to that of Chengdu. The city is a vast plain with the mountainous area in the west and hilly area in the east. The details are shown in TABLE I.

B. VIIRS Data

The Earth Observation Group in the National Oceanic and Atmospheric Administration's National Geophysical Data Center (NOAA/NGDC) of the United States released the monthly global NTL composite data from the VIIRS DNB. Data from August 2015 to December 2018 were downloaded (https://eogdata.mines.edu/download_dnb_composites.html) to analyze the relationship between NTL radiance and AOD. Each monthly tarball contained two files, namely, the average DNB radiance and the average number of cloud-free (NCF) observations. The 'vcmcfg' version of the data was used at a resolution of 15 arc-second (approximately 500 m) grids and radiance values with units in $nW \cdot cm^{-2} \cdot sr^{-1}$. These data were produced by averaging values of the DNB band after excluding data near the edges of the swath and data impacted by twilight, stray light, lightning, lunar illumination, and cloud-cover [44].

To estimate the aerosol effect on daily NTL radiance, the year 2016 was studied and data from NOAA Comprehensive Large Array-Data Stewardship System (CLASS) were downloaded. Four types of VIIRS data were used in this study: (a) VIIRS/DNB Sensor Data Record data (SVDNB), (b) VIIRS/DNB Geographical Sensor Data Record data (GDNBO), (c) VIIRS Cloud Aggregated Environment Data Record Ellipsoid Geolocation Environment Data Record data (GCLDO), and (d) VIIRS Cloud Cover Layers Environment Data Record data (VCCLO). The SVDNB data provided NTL radiation information. The GDNBO data provided corresponding geographic information for SVDNB radiance image. The GCLDO and VCCLO data were used to judge whether clouds would appear at night, so as to screen out the cloudless night. Each SVDNB radiance image had a swath of approximately 3060 km, which had been processed with radiometric calibration and stray light correction from raw DNB radiance data [45].

C. AERONET Aerosol Data

The AERONET observation instrument provides long-term AOD information in different regions of the world with an uncertainty lower than 0.02 [46]. Every 15 minutes, the AERONET measures the AOD of central wavelengths, which are 340, 380, 440, 500, 675, 870, 940, and 1020 nm. AOD data are available at three data quality levels (Levels 1.0, 1.5, and 2.0) and three temporal scales (15 min, daily, and monthly). Level 2.0 AOD data are processed with pre-field and post-field calibration, cloud screening, and quality control. In this study, Version 3 Level 2.0 AOD data with enhanced cloud screening and quality assurance [47] at the Beijing (39.98 N, 116.38 E) and Beijing CAMS (39.93 N, 116.32 E) sites are used to evaluate the aerosol effect on NTL, including daily data of 2016 and monthly data from August 2015 to December 2018. This study used the mean AOD of the two sites at 500 nm, which was consistent with Himawari products introduced in the following section.

This article has been accepted for publication in a future issue of this journal, but has not been fully edited. Content may change prior to final publication. Citation information: DOI 10.1109/JSTARS.2020.3003480, IEEE Journal of Selected Topics in Applied Earth Observations and Remote Sensing

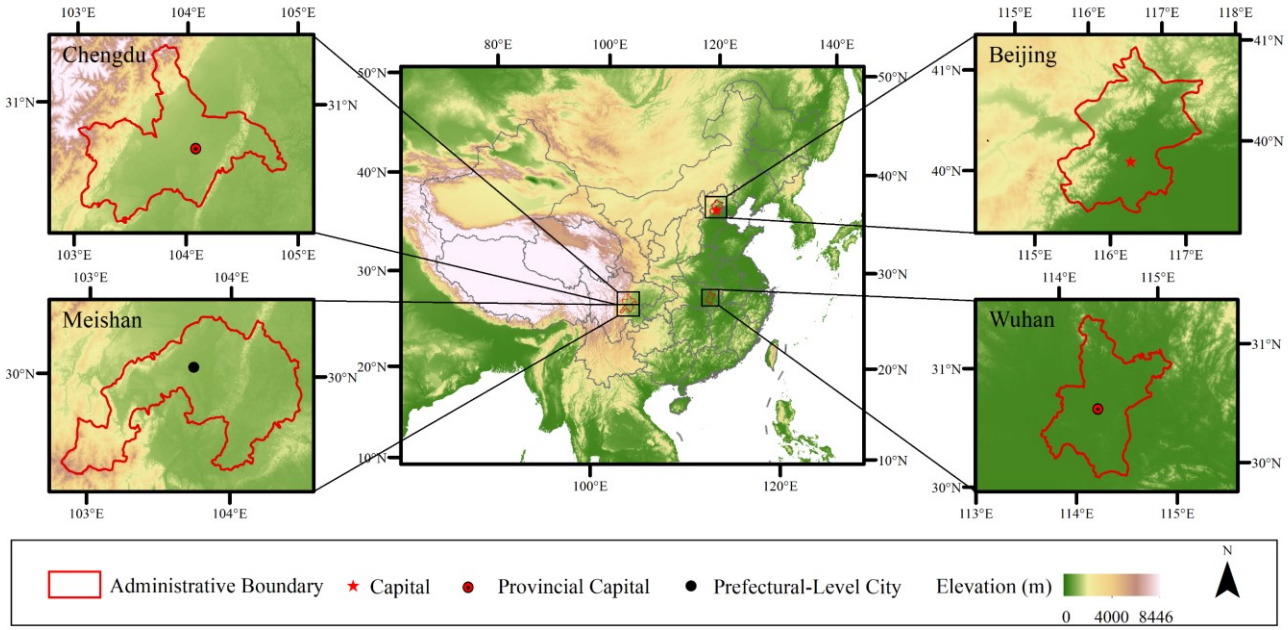

Fig. 1. Study areas.

TABLE I
INFORMATION OF STUDY AREAS

City	Land Area (km^2)	Average PM2.5 in 2015 ($\mu m/m^3$)	Urban Population (10000 persons)	Urbanization Rate [a] (%)	Climate
Beijing	16410.54	81	1876.6	86.45	Temperate semi-humid continental monsoon
Wuhan	8569.15	70	871.87	80.04	Subtropical humid southeast monsoon
Chengdu	14335	64	1152.81	71.85	Subtropical humid southeast and southwest monsoon
Meishan	7134	62	133.18	44.77	Similar to that of Chengdu

[a] The proportion of the urban population to the total population. Data are obtained from statistical yearbook for 2017 of four cities.

D. Himawari Aerosol Products

Himawari-8 is a new-generation meteorological satellite launched by the Japan Meteorological Agency (JMA) on 7 October 2014. The Advanced Himawari Imager (AHI) has a wide range of wavelengths, including 16 bands from visible to infrared wavelengths and 10 min observation frequency of full disk [48]. This satellite also provides 10 min, hourly, daily, and monthly variability of AOD over Asia and Oceania. In this study, Level 3 Version 3 daily and monthly AOD are downloaded from https://www.eorc.jaxa.jp/ptree/terms.html. The resolution of the AOD is 0.05° at a wavelength of 500 nm, and the subdataset named AOT_L2_Mean are used. Detailed information about the products can be found in the document(https://www.eorc.jaxa.jp/ptree/documents/Himawari_Monitor_Aerosol_Product_v5.pdf).

Beijing, as a highly urbanized capital city, generally attracts high public attention and its AOD-related data are the most abundant among the four cities. Quantitative analyses of NTL radiance and AOD in Beijing are conducted with daily and monthly data. By contrast, the other three cities have no AERONET sites as yet, and thus are analyzed using monthly Himawari AOD. Since only daytime AOD can be obtained from ARONET and Himawari, the AOD of two successive days (before and after VIIRS nighttime overpass) were averaged for analysis.

III. METHODS

A. Data Preprocessing

All the spatial data (including remotely sensed and administrative boundary data) were resampled to the same spatial resolution as VIIRS DNB monthly composites (0.0041667°). The daily NTL radiance data that did not contain all of Beijing were excluded. Unlike the well-processed monthly NTL data produced by NOAA/NGDC, daily NTL data were checked using the following flowchart, as shown in Fig. 2.

1) Step 1: The solar zenith angle (SZA) information from the GDNBO product was extracted, and the NTL radiance data with SZA < 101° were discarded to remove the impact of sunlight [33]. To exclude NTL images contaminated by moonlight, the local moonrise and moonset time information (https://sunrisesunsetmap.com) were used and then the data without moonlight contamination were selected.

2) Step 2: Cloud cover data were extracted using the VCCLO. According to these data, clouds were masked and then NTL radiance data without sunlight, clouds, and bad data were selected.

3) Step 3: The VIIRS can revisit a place more than once

This article has been accepted for publication in a future issue of this journal, but has not been fully edited. Content may change prior to final publication. Citation information: DOI 10.1109/JSTARS.2020.3003480, IEEE Journal of Selected Topics in Applied Earth Observations and Remote Sensing

every night because of the design of the satellite orbit. Two NTL images acquired in the same area within one night were combined by average to acquire the daily processed data. Similarly, the satellite viewing zenith angle (VZA) extracted from GDNBO was also processed using Steps 1 and 2. In addition, Himawari daily AOD at the urban center of Beijing in 2016 were masked according to the corresponding NTL images to ensure the regional consistency in subsequent analysis. The masked daily AOD with less than 1000 pixels were excluded.

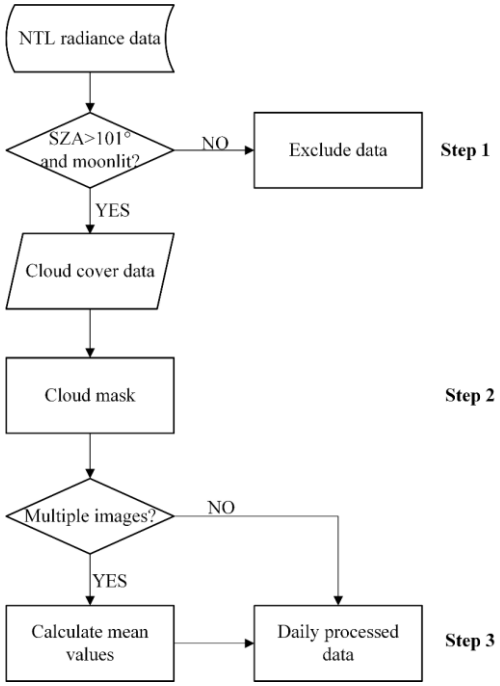

Fig. 2. Flowchart for checking the daily NTL radiance data.

B. Extraction of Urban Centers

With dense buildings, well-developed transportation, and more human activities, urban centers are illuminated artificially at night, and their corresponding pixels in NTL images have larger radiance values than the surrounding suburban countryside. Moreover, urban expansion is generally centered on the old city, which has not changed significantly over time. The local overpass time of the NPP satellite at night is approximately 1:30 AM when most of the residential indoor lights have been turned off. The main light sources are the street and infrastructure lights, which may not change much with time [49], and thus the light background value of this area can be assumed to remain the same.

Shi *et al.* [18] extracted the built-up urban areas with the light synthesis data of 2012 (18–26 April 2012 and 11–23 October 2012) and obtained the light thresholds of different cities (TABLE II). This study extracts the urban centers based on these thresholds. The details of the processes are described below.

1) Acquisition of urban pixels: Any pixel in the monthly light synthesis data of April 2012 with radiance exceeding the threshold was identified as a city pixel. After threshold screening, areas with fragments were obtained.

2) Region of interest (ROI) extraction: Small fragments were deleted and the largest zone was retained. Several small void pixels (one or several pixels were not selected) were placed in the zone and vector boundaries were obtained for urban centers of four cities, as shown in Fig. 3.

3) NTL data of urban centers: Using vector files to extract all the NTL images, a series of urban center NTL data were obtained. Similarly, NCF, Himawari daily AOD, Himawari monthly AOD data, and 10-m-resolution land cover data [50] were masked using vector files. TABLE II shows the NTL data acquired at the four urban centers (April 2012) and the proportions of impervious surface (2017). Fig. 3 shows the extraction results of the urban centers of four cities, among which the urban center of Beijing is the largest and that of Meishan is the smallest. The proportions of the impervious surface of four cities are all approximately 70%.

4) The regional average radiance (I) and logarithm of the radiance [$ln(I)$] for all the NTL radiance data of urban centers were calculated. Furthermore, regional average values of NCF data were calculated, and monthly NTL data with values lower than 3 were discarded.

C. Statistical Analysis of NTL Radiance Distribution

Anomaly is the deviation of a value from the mean of a dataset. Based on the mean value of the daily AOD of Beijing in 2016, the AOD anomaly (AOD_d) was calculated. According to the AOD_d range, aerosol pollution was divided into five levels (Level-1 to 5), that is, relatively clean, lightly polluted, moderately polluted, heavily polluted, and severely polluted. Then, the box plot, also known as box-whisker plot, was applied to measure the NTL radiance distribution according to the graded AOD. Box plot describes data using its five statistics: minimum, first quartile, median, third quartile, and maximum.

D. Modeling the Aerosols Effect

The relationship between the NTL radiance and AOD is analyzed using two models, namely, Linear Regression (LR) and Log-linear Regression (L-LR). The ordinary least squares algorithm is widely used to fit the regression models. The LR model is:

$$I = a\tau + b, \tag{1}$$

where I is the radiance that the DNB sensor received, τ is the total optical depth, and a and b are the coefficients. τ consists of Rayleigh scattering optical depth (τ_{ray}), unscreened cirrus optical depth (τ_c) and aerosol optical depth (τ_{aer}). We assume that τ_{ray} is relatively stable and VIIRS DNB data are cloud-free after cloud mask. Thus τ is equivalent to τ_{aer}.

If the effects of cloud and moonlight are removed, the radiance received by the satellite sensor only includes part of the ground light source. Ignoring the contributions from multiple scattering effects and considering the differences of viewing geometries between various nights, the relationship between τ and I can be expressed in the following formula [19, 23]:

This article has been accepted for publication in a future issue of this journal, but has not been fully edited. Content may change prior to final publication. Citation information: DOI 10.1109/JSTARS.2020.3003480, IEEE Journal of Selected Topics in Applied Earth Observations and Remote Sensing

TABLE II
REGIONAL SCREENING CRITERIA AND RESULTS OF DIFFERENT CITIES

City	Beijing	Wuhan	Chengdu	Meishan
Light Threshold ($nW{\cdot}cm^{-2}sr^{-1}$)	14.145	16.88	21.7	10.41
Mean Value of Urban Area ($nW{\cdot}cm^{-2}sr^{-1}$)	27.035	26.329	36.793	16.722
Pixel Counts	7044	2271	2134	104
Proportion of Impervious Surface (%)	66.41	75.55	75.50	69.70

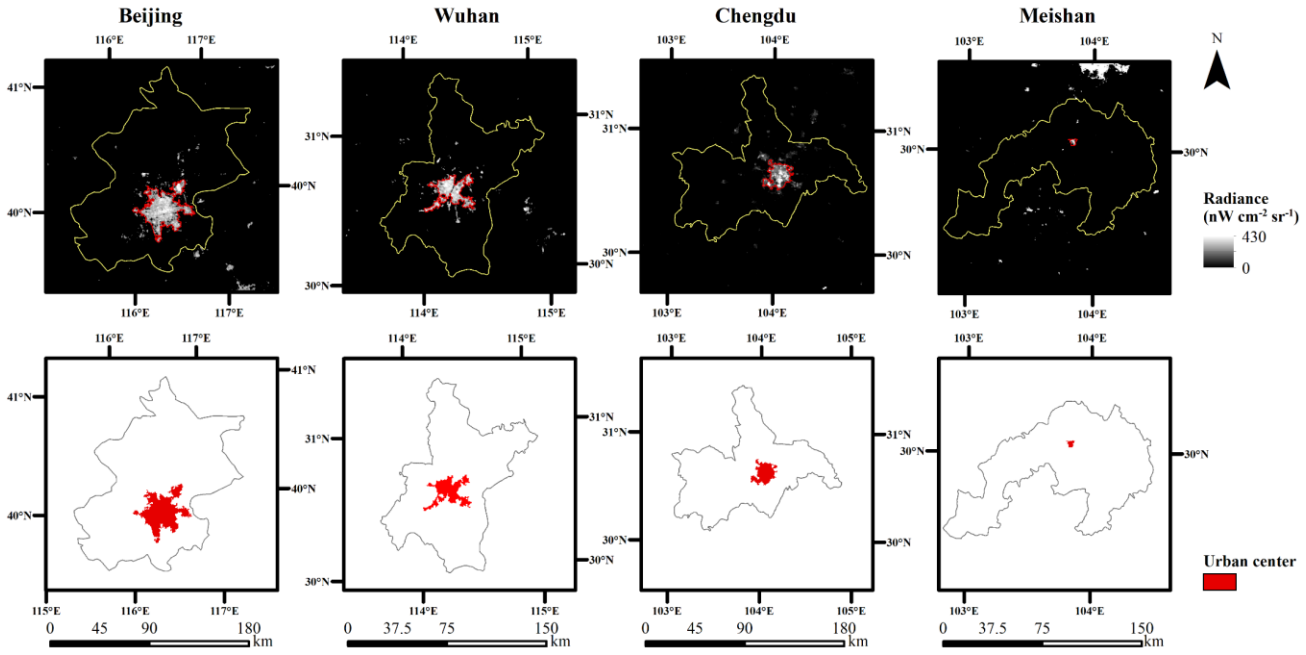

Fig. 3. Urban centers of four cities.

$$I = I_0 e^{-\tau/\mu}, \quad (2)$$

where I_0 is the initial (unattenuated) upwelling radiance from the surface light source (artificial light) and μ is the cosine of the VZA. Then, a simplified radiation transfer equation (L-LR) is made:

$$ln(I) = a\tau + b. \quad (3)$$

Eq. (1) is approximately equivalent to Eq. (3) when a is small.

The effect of VZA on NTL data is also analyzed using a more complicated model. Li *et al.* [51] discovered the relationship between the artificial light radiance and satellite viewing angles by using the daily NTL images and used a quadratic model as in Eq. (4) to remove this impact. Combining Eqs. (2) and (4), a model is reconstructed to jointly consider VZA and AOD,

$$I_0 = a\theta^2 + b\theta + c, \quad (4)$$

$$I = (a\theta^2 + b\theta + c)e^{d\tau/\cos(\theta)}, \quad (5)$$

where θ denotes the VZA and a, b, c, and d are the coefficients.

IV. RESULTS

A. Time Series of NTL Radiance and AOD

Fig. 4 shows the monthly series change of NTL radiance and AOD of four cities. Beijing's monthly NTL composites of May, June, and July are missing due to poor data quality. The monthly series image shows that the NTL radiance and AOD generally show an opposite change trend. The minimum radiance values for Beijing and Wuhan are in November 2015, while those of Chengdu and Meishan are in December 2018 and January 2018, respectively.

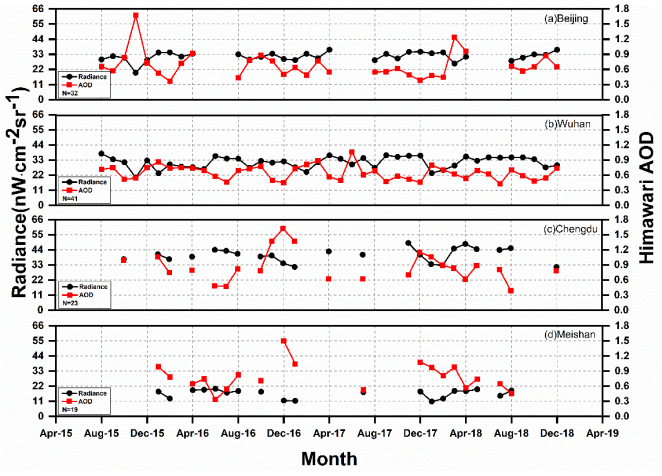

Fig. 4. Monthly series of NTL radiance and AOD for the four cities: (a) Beijing (b) Wuhan (c) Chengdu (d) Meishan.

This article has been accepted for publication in a future issue of this journal, but has not been fully edited. Content may change prior to final publication. Citation information: DOI 10.1109/JSTARS.2020.3003480, IEEE Journal of Selected Topics in Applied Earth Observations and Remote Sensing

As is shown in Fig. 5, the relationship among monthly mean NTL radiance of four urban centers is Chengdu > Wuhan > Beijing > Meishan, and that among the Himawari AOD is Chengdu > Meishan > Beijing > Wuhan. The ranges of NTL radiance are 19.6–36.3 $nW{\cdot}m^{-2}sr^{-1}$, 20.3–37.6 $nW{\cdot}m^{-2}sr^{-1}$, 31.4–48.9 $nW{\cdot}m^{-2}sr^{-1}$, and 10.8–20.1 $nW{\cdot}m^{-2}sr^{-1}$ for Beijing, Wuhan, Chengdu, and Meishan, respectively. All variation ranges of NTL radiance are higher than 15 $nW{\cdot}m^{-2}sr^{-1}$ except for that of Meishan. The ranges of monthly AOD are 0.368–1.67, 0.427–1.06, 0.386–1.62, and 0.334–1.50 for Beijing, Wuhan, Chengdu, and Meishan, respectively. The variation ranges of AOD are larger than 1 except for that of Wuhan.

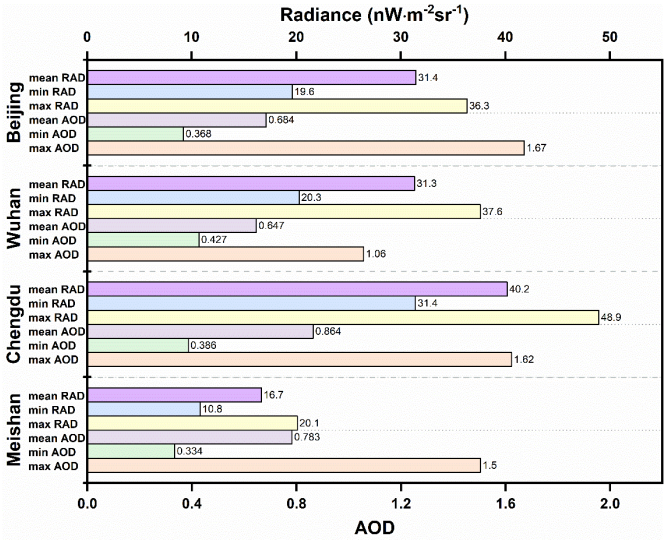

Fig. 5. Statistics of monthly NTL radiance and Himawari AOD information of the four cities. RAD represents the NTL radiance.

Fig. 6 shows the monthly series change of NTL radiance and AOD in Beijing. Both AERONET and Himawari AOD exhibit negative correlations with NTL radiance. The lowest radiance value is in December 2015, and the corresponding AOD is the largest. From the second half of 2015 to the first half of 2016, the NTL radiance of Beijing shows considerable fluctuations. The NTL radiance distinctly increases especially from November 2015 to February 2016. Fig. 6 shows that the change trends of the two types of AOD are similar, although Himawari AOD is generally higher than AERONET AOD. Further analysis shows that the similar result of the daily comparison of AERONET and Himawari AOD in Beijing and R^2 is 0.743 and the Root Mean Squared Error (RMSE) is 0.447 (Fig. 7). R^2 and RMSE are both higher than those in Zhang *et al.* [52].

B. Analysis of NTL Radiance and AOD of Beijing

Based on the average value of the daily AOD of Beijing in 2016, the AOD_d, i.e., the deviation from the average, is adopted to represent the change of AOD and air cleanliness. The ranges of AOD_d are within −0.7 ~ 0.7 except for a few larger values. Therefore, the AOD_d is divided into five levels according to the criteria shown in TABLE III.

To illustrate the effect of AOD on NTL radiance, the box plot is applied to show the variation of NTL radiance distribution among different AOD levels. The results are derived using AERONET and Himawari AOD, as shown in Fig. 8. The "box" including its inner line, solid circle, and whisker has a significant change at different AOD_d levels. As the AOD increases (from Level-1 to Level-5), the mean and median decrease, which suggests an opposite trend between NTL radiance and aerosols. The 75th percentile Fig. 8(a) and the 25th percentile of Fig. 8(b) also show a similar trend to the mean. The box sizes for Fig. 8(a) and Fig. 8(b) vary because of the difference between the two AOD products.

The relationship of daily NTL radiance and AOD is shown in scatter plots (Fig. 9). The radiance decreases with the increase of AOD for both AERONET and Himawari. The R^2 values of 0.381 and 0.493 are obtained using the LR model for AERONET and Himawari, respectively ($P < 0.01$). The R^2 of 0.421 and 0.576 are obtained using the L-LR model for AERONET and Himawari, respectively ($P < 0.01$).

The monthly analysis was carried out for the aerosol effects on NTL data. Fig. 10 shows the relationship between NTL radiance and AOD by fitting with the LR and L-LR models.

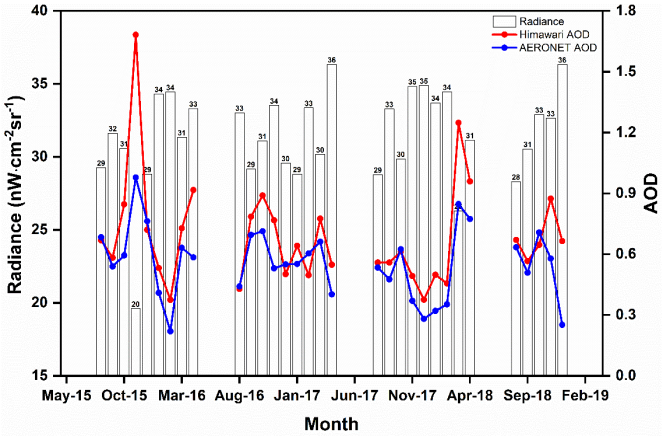

Fig. 6. Monthly change of NTL radiance and AOD in Beijing. The red and blue lines represent the monthly Himawari AOD and AERONET AOD, respectively. The NTL radiance is shown with the histogram.

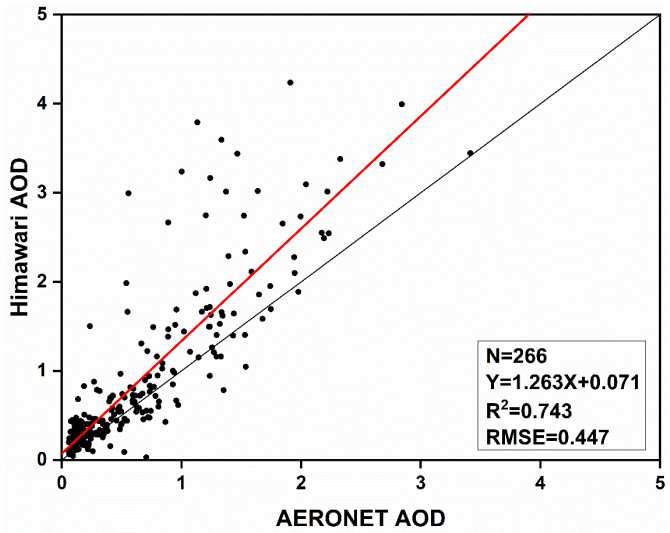

Fig. 7. Comparison of daily Himawari and AERONET AOD (Beijing CAMS site) in 2016. The red and black lines represent the linear trend line and the 1:1 line, respectively.

This article has been accepted for publication in a future issue of this journal, but has not been fully edited. Content may change prior to final publication. Citation information: DOI 10.1109/JSTARS.2020.3003480, IEEE Journal of Selected Topics in Applied Earth Observations and Remote Sensing

TABLE III
GRADED AOD ANOMALY FOR BEIJING

AOD_d range	Air pollution level	Defined pollution level
$AOD_d \leq -0.4$	Relatively clean	Level-1
$-0.4 < AOD_d < -0.1$	Lightly polluted	Level-2
$-0.1 \leq AOD_d < 0.1$	Moderately polluted	Level-3
$0.1 \leq AOD_d < 0.4$	Heavily polluted	Level-4
$AOD_d \geq 0.4$	Severely polluted	Level-5

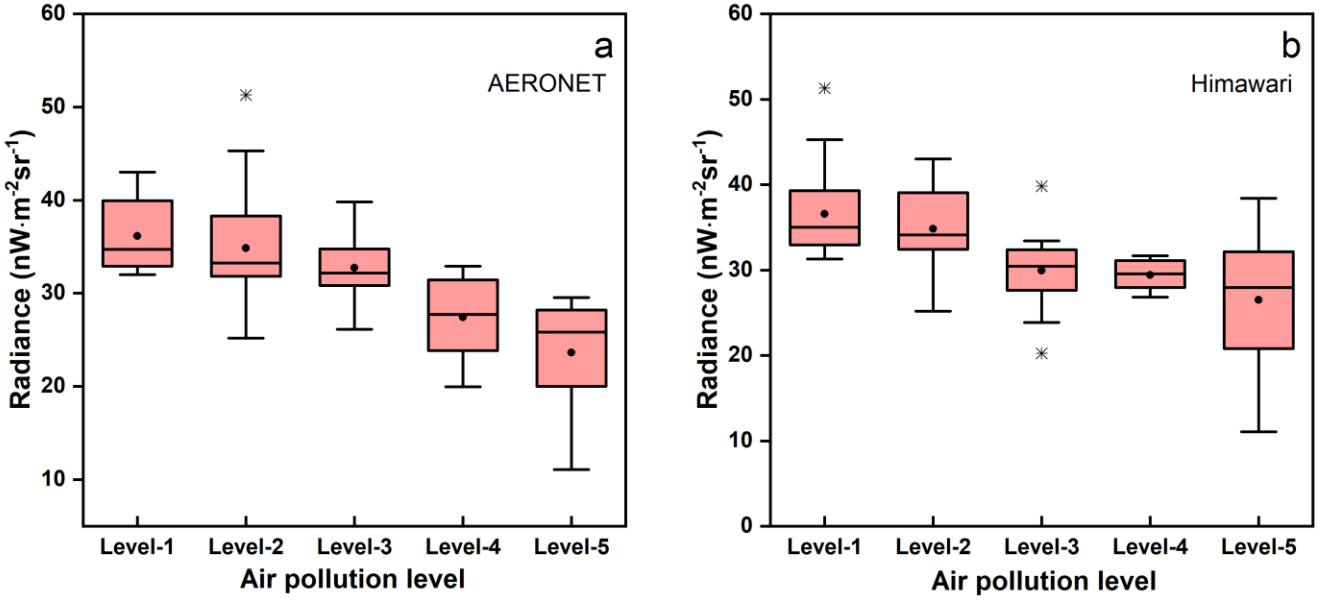

Fig. 8. Box plots of daily NTL radiance against graded air pollution level: (a) AERONET (b) Himawari. For each level, the following descriptive statistics are shown: minimum, 25th quartile, median, mean, and 75th quartile with the limits (ends of the "whiskers") beyond which values are considered anomalous (displayed as black stars). The mean is displayed with a black dot, and a black line (in the middle of the box) corresponds to the median.

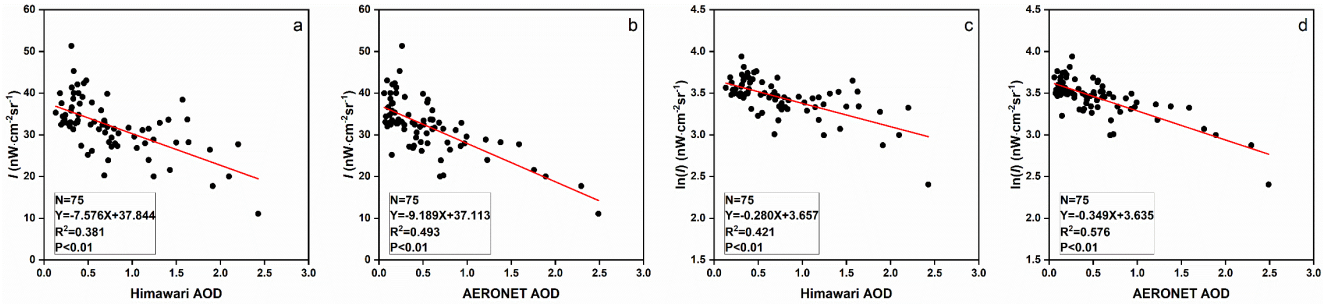

Fig. 9. Relationship of daily NTL radiance and AOD in Beijing. (a, b) using LR regression model and (c, d) using L-LR regression model. The red lines denote the trend lines.

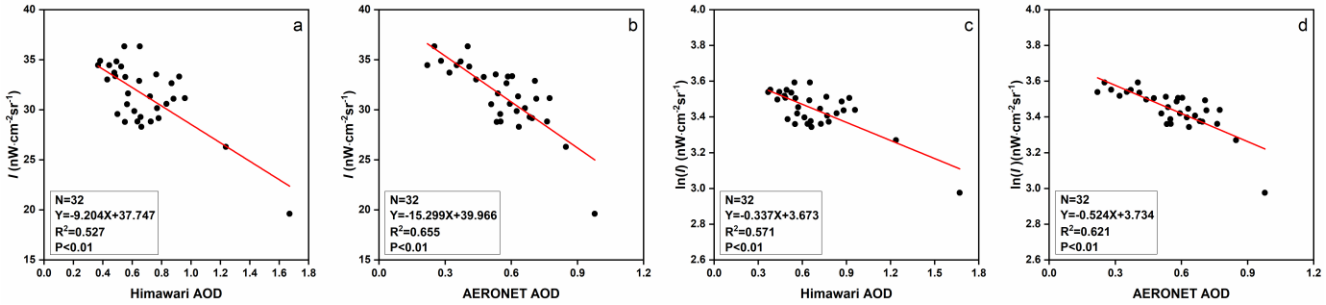

Fig. 10. Relationship of monthly NTL radiance and AOD in Beijing. (a, b) using LR regression model and (c, d) using L-LR regression model. The red lines denote the linear trend lines.

This article has been accepted for publication in a future issue of this journal, but has not been fully edited. Content may change prior to final publication. Citation information: DOI 10.1109/JSTARS.2020.3003480, IEEE Journal of Selected Topics in Applied Earth Observations and Remote Sensing

TABLE IV
RELATIONSHIP BETWEEN NTL RADIANCE AND AOD OF BEIJING

Model	AOD Product	Time Scale	r	R^2	a	b
LR	AERONET	Daily	−0.702*	0.493	−9.189	37.113
	Himawari	Daily	−0.617*	0.381	−7.576	37.844
	AERONET	Monthly	−0.809*	0.655	−15.299	39.966
	Himawari	Monthly	−0.726*	0.527	−9.204	37.747
L-LR	AERONET	Daily	−0.759*	0.576	−0.349	3.635
	Himawari	Daily	−0.649*	0.421	−0.280	3.657
	AERONET	Monthly	−0.788*	0.621	−0.524	3.734
	Himawari	Monthly	−0.756*	0.571	−0.337	3.673

"*" denotes that correlation is significant at 0.01 level.

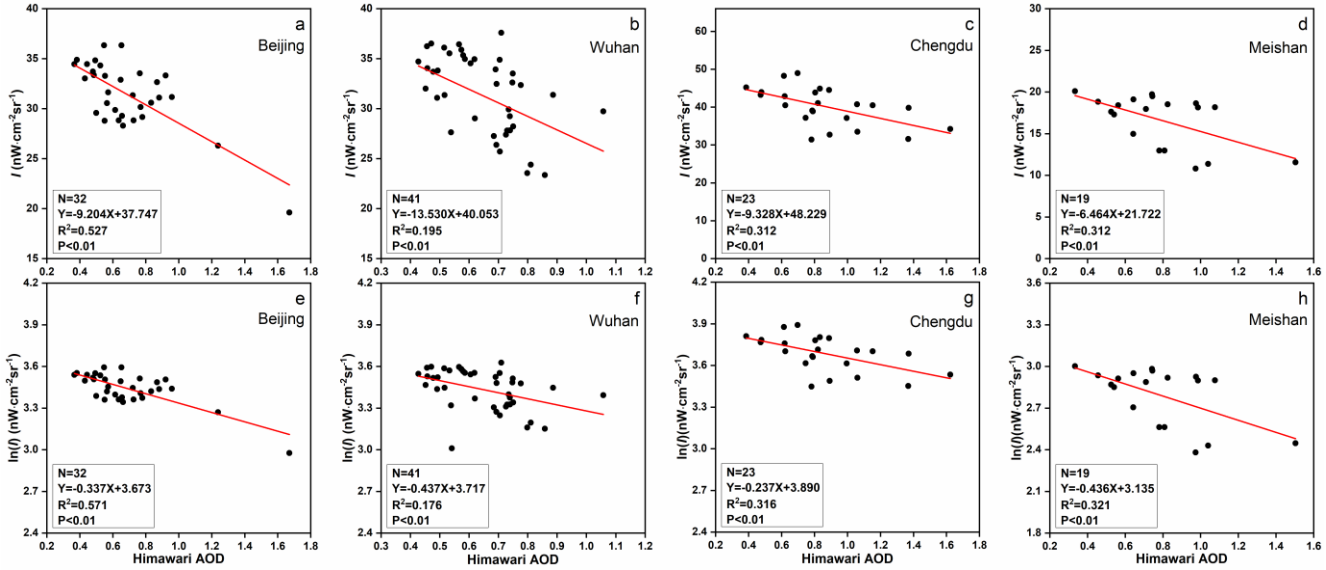

Fig. 11. Scatter plots of radiance and Himawari AOD using the LR model (a, b, c and d) and the L-LR model (e, f, g and h) for the four cities.

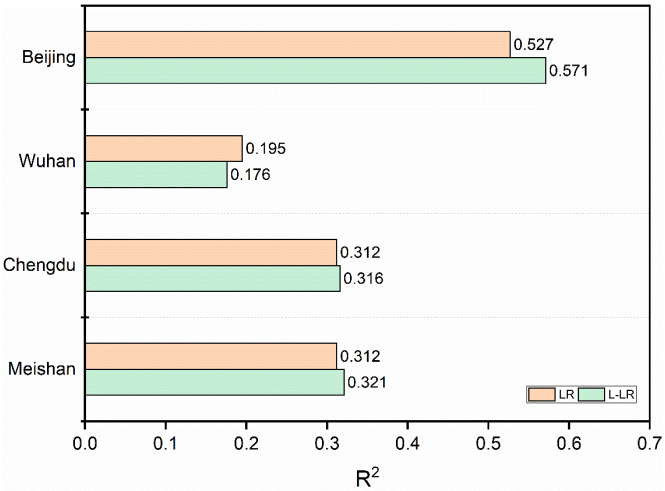

Fig. 12. R^2 values of LR and L-LR models for the four cities.

NTL radiance decreases as AOD increases. The R^2 values of 0.527 and 0.655 are obtained using the LR model for Himawari AOD and AERONET AOD, respectively. R^2 changes less than 0.05 by using the L-LR model. The results are statistically significant ($P < 0.01$), and show that the relationship between NTL radiance and AOD is quasi-linear.

TABLE IV shows the Pearson correlation coefficient (r) and the corresponding coefficients a and b. The r values are lower than −0.61 and verified the negative correlation between NTL radiance and AOD. The results using the L-LR model are almost slightly larger than those obtained using the LR model, suggesting that the simplified radiation transfer equation can slightly better represent the relationship between the NTL radiance and AOD. For the LR model, the slope (a) of the linear function for Himawari AOD is less than that for AERONET AOD, indicating their difference (Fig. 7, Himawari AOD overall is larger than AERONET AOD). Monthly a values are larger than daily a values. In general, the b values are almost consistent for each model.

C. *Comparative Analysis of Different Cities*

The LR and the L-LR models are used to fit the NTL radiance and AOD of the four urban centers. As shown in Fig. 11, the order of a values is Wuhan (13.530) > Chengdu (9.328) > Beijng (9.204) > Meishan (6.464) for the LR model, and Wuhan (0.437) > Meishan (0.436) > Beijng (0.337) > Chengdu (0.237) for the L-LR model. The order of b values in LR and L-LR models is Chengdu (48.229, 3.890) > Wuhan (40.053, 3.717) > Beijng (37.747, 3.673) > Meishan (21.722,

This article has been accepted for publication in a future issue of this journal, but has not been fully edited. Content may change prior to final publication. Citation information: DOI 10.1109/JSTARS.2020.3003480, IEEE Journal of Selected Topics in Applied Earth Observations and Remote Sensing

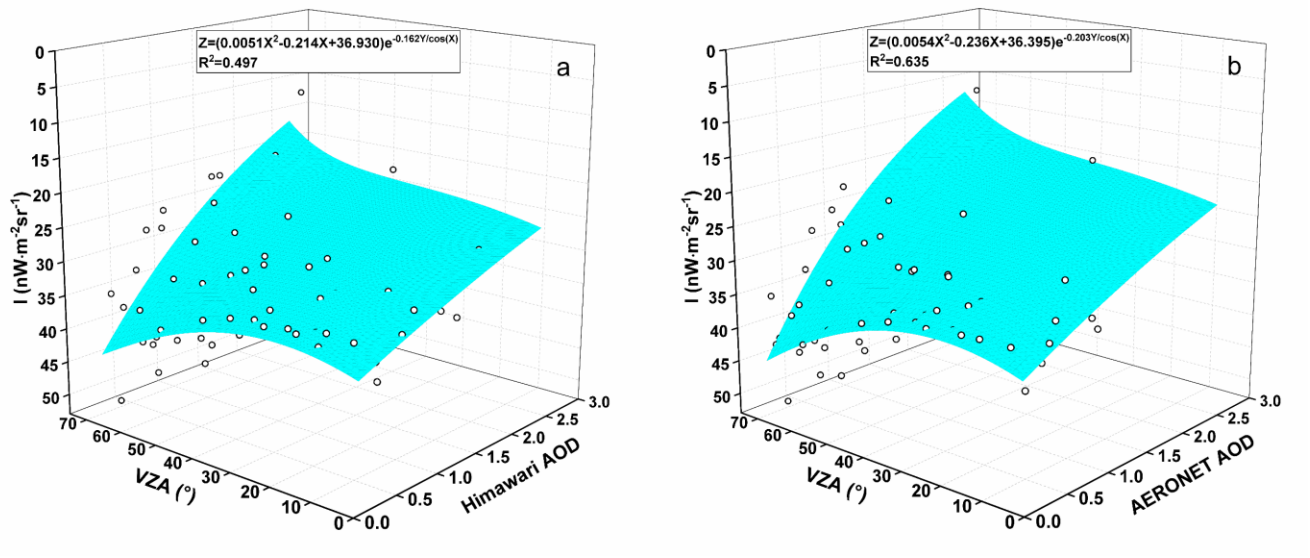

Fig. 13. Fitting of NTL radiance, VZA, and AOD. (a) Himawari AOD, (b) AERONET AOD. The blue surfaces are fitted using Eq.(5). X, Y, and Z represent VZA, AOD, and NTL radiance, respectively.

3.135) which is similar to the order of the threshold used to determine the urban centers (TABLE II). Fig. 12 shows similar R^2 values for the two models, whereas the R^2 value in each urban center varies significantly. For example, the R^2 obtained using the L-LR model for Beijing is 0.571 while that for Wuhan is 0.176.

D. Influence of Anisotropic Effect

Daily NTL radiance is obtained at a specific viewing angle, which changes every day. Eq. (5) is used to describe the joint effects of VZA and AOD on NTL radiance with the daily data acquired in Beijing, as shown in Fig. 13. As the AOD increases, NTL radiance decreases. In addition, the NTL radiance is relatively high when VZA is large. The R^2 values are 0.497 and 0.635 for Himawari AOD and AERONET AOD, respectively, and are slightly larger than those using the L-LR model (0.421 and 0.576 in TABLE IV), suggesting that the consideration of VZA slightly improves the correlation between daily NTL radiance and AOD. The coefficient d of the two equations in Eq. (5) Fig. 13 are almost the same as b values in LR model (about 37 in TABLE IV) and can also express the unattenuated upwelling radiance from the surface light source I_0.

V. Discussion

A. Potential Impact of AOD on Application of NTL Data

The VIIRS DNB data can be used in feature detection, fire monitoring, urban expansion research, and population estimation, which all need thresholds to recognize and discriminate NTL of different areas. These thresholds are easily affected by aerosols in the atmosphere and may show a blooming effect strengthened by the scattering of aerosol particles in VIIRS DNB data [53]. In this study, quantitative analyses are carried out on the relationships of NTL radiance and AOD in Beijing and three other cities of different development stages. The relationship between NTL radiance and AOD suggests that the radiance may decrease by over 15 $nW{\cdot}cm^{-2}sr^{-1}$ when AERONET AOD increases one unit (for Beijing in TABLE IV). This amount is higher than the threshold of urban areas (14.145 $nW{\cdot}cm^{-2}sr^{-1}$) obtained using published methods [18], indicating the considerable atmospheric effect on NTL data. Eqs. (1) and (3) indicate that the coefficient b in the LR model and e^b in the L-LR model are in essence the initial upwelling radiance from the surface light source I_0 and a represents the sensitivity of the NTL radiance to AOD. The upwelling radiance from the surface light source highly varies among cities (the NTL radiance of Meishan is half as those of others in Fig. 4). By contrast, the slope a is the second largest for Meishan among the four cities using the L-LR model (Fig. 11), showing that the sensitivity of NTL radiance to AOD is relatively independent to the initial upwelling NTL radiance. Therefore, the regression coefficients constructed with AOD are potentially valuable in the correction of atmospheric effects in NTL data.

B. Other Related Factors

The relationship between the NTL radiance and AOD are also affected by several factors, including the temporal and spatial characteristics of data, types of AOD, and regression models.

1) Time scale of data

The R^2 of monthly results are higher than that of daily results in TABLE IV. Although the VIIRS DNB data released by NOAA has undergone geometric correction, radiometric calibration, and stray light removal [45], numerous factors influence the uncertainty of the daily NTL data compared with the monthly NTL data. Li *et al.* [51] analyzed the relationship between the radiance and satellite viewing angles using the daily NTL images. Both I and I_0 are functions of VZA. Given the periodicity of the satellite orbit, the monthly NTL data tend to mitigate the angle effect. Another reason is the existence of statistical deviations. The data of low polluted

This article has been accepted for publication in a future issue of this journal, but has not been fully edited. Content may change prior to final publication. Citation information: DOI 10.1109/JSTARS.2020.3003480, IEEE Journal of Selected Topics in Applied Earth Observations and Remote Sensing

atmosphere have high data quality and are prone to be selected, causing the daily datasets to mainly concentrate on low AOD values (Fig. 9). Monthly aggregation increases the uniform distribution of AOD data, which may enhance the correlation between NTL radiance and AOD.

2) Difference of cities

The NTL radiance values of Beijing, Wuhan, and Chengdu are similar, but that of Meishan is much lower. Given the rainy weather in Chengdu and Meishan, less NTL composite data are available than those for Beijing and Wuhan. The R^2 value of Wuhan is less than the other three cities, and the largest is for Beijing (Fig. 12). The AOD level for Wuhan is the lowest among the four cities (Fig. 5), resulting in a weak correlation between the NTL radiance and AOD. Beijing is located in a basin, promoting the accumulation of air pollutants and limiting their dispersion. Similarly, Chengdu and Meishan are located in the Sichuan Basin, which is also not conducive to the diffusion of pollutants. Thus, the NTL radiance change caused by AOD is more prominent and the correlation is higher. In fact, the DNB band (500–900 nm) contains the effect of water vapor absorption that thereby affects the a values. Compared with the other three cities, Beijing is relatively dry and the influence of water vapor is smaller. The a values of the three large cities are higher than that of Meishan, as shown in Fig. 11(a-d), suggesting that AOD may have greater impact on the NTL radiance of cities with high urbanization levels. The results imply that the relationship between NTL radiance and AOD varies among cities of different urbanization levels and climate types.

3) Different AOD products

We can see from TABLE IV that the slope value a derived from NTL radiance and Himawari AOD is generally smaller than that derived from NTL radiance and AERONET AOD. This is caused by the overestimation of Himawari AOD as shown in Fig. 6-Fig. 7, also in agreement with Zhang *et al.* [52]. The AOD of AERONET is more reliable than Himawari AOD, therefore the regression relationship obtained by AERONET is relatively more accurate. Future updates on aerosol retrieval methods with satellite data can help promote the fitting accuracy of NTL data and AOD.

4) Difference of regression models

Fig. 12 and TABLE IV show that the R^2 values obtained using the L-LR model are slightly larger than those obtained using the LR model (the improvement is less than 0.05), suggesting that the simplified radiation transfer equation Eq. (2) can slightly better represent the relationship between NTL radiance and AOD. In essence, this relationship is logarithmic, and is also used to retrieve AOD [19, 20, 23, 54]. However, a description with linear fitting is simpler and can largely reflect the relationship.

C. Limitations

In this study, the LR model is used to analyze the relationship between NTL radiance and AOD. The Pearson correlation coefficient of Beijing is approximately 0.8, yet this value is not very high overall and even smaller for other cities, suggesting that aerosols cannot account for all the radiance changes in urban centers. The possible reasons are as follows: (1) The daytime AOD used in this study may have a certain difference with nighttime AOD [55]; (2) The NTL background values of urban centers are assumed to be unchanged with time because the NTL data were obtained at midnight when human activities are reduced. Uncertainties also exist, such as socio-economic development or extreme short-term events [28]; (3) The changes of land cover can result in seasonal changes of NTL radiance in the long term [56]. Although the urban centers extracted are mostly covered by impervious surface (TABLE II), vegetation changes influence the NTL radiance, especially in Beijing that has deciduous forests with four distinct seasons; (4) The VIIRS DNB data contains information in a wide range of wavelength from 500–900 nm, where the oxygen A-band and other absorbing bands such as water vapor [19]; (5) Uncertainty caused by unscreened cirrus cloud is ignored. Passive radiometric satellite products are contaminated by cirrus cloud about 25% of the time [57]. Unscreened cirrus cloud may cause radiance attenuation in the NTL data.

D. Suggestions for future work

In view of the factors mentioned above, several improvements can be used in future research. First, nighttime atmospheric data observed from CALIPSO [58] and the new sun-sky-lunar Cimel CE318-T multiband photometer [59] can be used to analyze the relationship between nighttime aerosols and NTL radiance. Second, the impact of short-term events and long-term seasonal changes of both AOD and NTL data need consideration. Third, although the AERONET AOD represents the ground truth and the accuracy is high, the spatial representation of sites remains to be discussed. Finally, more cities are needed to reveal the aerosol effect on NTL radiance and the feasibility of using the AOD data to remove the atmospheric effect on NTL data.

VI. Conclusions

The change of NTL radiance contains signals of air pollution, which influence the quantitative application of NTL data. The atmospheric effect requires consideration and corresponding correction are necessary before the application of NTL data. Two regression models are applied to detect the relationship between NPP-VIIRS NTL radiance and AOD of AERONET and Himawari. The results suggest that changes in NTL radiance are negatively correlated with changes of AOD for urban centers of four different cities in China. The correlation is strongest in Beijing, where high Pearson correlation coefficient (approximately −0.8) was obtained in monthly analysis. The NTL radiance may decrease by 10 $nW \cdot cm^{-2}sr^{-1}$ as the daily AERONET AOD increases by one unit. This decrease may reach above 15 $nW \cdot cm^{-2}sr^{-1}$ for monthly AERONET AOD. The comparison shows the influence of AOD in cities with different sizes, climate types, and development stages. This influence is prominent for cities with high urbanization level and dry climate.

ACKNOWLEDGEMENTS

The authors are grateful for the monthly global NTL composite data from the VIIRS DNB provided by the Earth Observation Group of Payne Institute, VIIRS data provided by NOAA Comprehensive Large Array-Data Stewardship System, H8/AHI data provided by Japan Aerospace Exploration Agency, and AERONET data maintained by Institute of Atmospheric Physics, Chinese Academy of Sciences (Beijing site), and Chinese Academy of Meteorological Science (CMAS site).

REFERENCES

[1] M. M. Bennett and L. C. Smith, "Advances in using multitemporal night-time lights satellite imagery to detect, estimate, and monitor socioeconomic dynamics," *Remote Sensing of Environment,* vol. 192, pp. 176-197, 2017.

[2] C. D. Elvidge, K. E. Baugh, M. Zhizhin, and F. C. Hsu, "Why VIIRS data are superior to DMSP for mapping nighttime lights," *Proceedings of the Asia-Pacific Advanced Network,* vol. 35, p. 62, 2013.

[3] L. Coscieme, F. M. Pulselli, S. Bastianoni, C. D. Elvidge, S. Anderson, and P. C. Sutton, "A thermodynamic geography: night-time satellite imagery as a proxy measure of emergy," *Ambio,* vol. 43, pp. 969-79, Nov 2014.

[4] T. Ma, C. Zhou, T. Pei, S. Haynie, and J. Fan, "Responses of Suomi-NPP VIIRS-derived nighttime lights to socioeconomic activity in China's cities," *Remote Sensing Letters,* vol. 5, pp. 165-174, 2014.

[5] X. Chen and W. Nordhaus, "A test of the new VIIRS lights data set: Population and economic output in Africa," *Remote Sensing,* vol. 7, pp. 4937-4947, 2015.

[6] Z. Chen, B. Yu, Y. Hu, C. Huang, K. Shi, and J. Wu, "Estimating house vacancy rate in metropolitan areas using NPP-VIIRS nighttime light composite data," *IEEE Journal of Selected Topics in Applied Earth Observations and Remote Sensing,* vol. 8, pp. 2188-2197, 2015.

[7] K. Shi, B. Yu, Y. Hu, C. Huang, Y. Chen, Y. Huang, *et al.*, "Modeling and mapping total freight traffic in China using NPP-VIIRS nighttime light composite data," *GIScience & Remote Sensing,* vol. 52, pp. 274-289, 2015.

[8] B. Yu, K. Shi, Y. Hu, C. Huang, Z. Chen, and J. Wu, "Poverty evaluation using NPP-VIIRS nighttime light composite data at the county level in China," *IEEE Journal of Selected Topics in Applied Earth Observations and Remote Sensing,* vol. 8, pp. 1217-1229, 2015.

[9] N. Levin and Q. Zhang, "A global analysis of factors controlling VIIRS nighttime light levels from densely populated areas," *Remote sensing of environment,* vol. 190, pp. 366-382, 2017.

[10] C. Elvidge, M. Zhizhin, K. Baugh, and F.-C. Hsu, "Automatic Boat Identification System for VIIRS Low Light Imaging Data," *Remote Sensing,* vol. 7, pp. 3020-3036, 2015.

[11] C. Hu, S. Chen, M. Wang, B. Murch, and J. Taylor, "Detecting surface oil slicks using VIIRS nighttime imagery under moon glint: a case study in the Gulf of Mexico," *Remote Sensing Letters,* vol. 6, pp. 295-301, 2015.

[12] W. Straka, C. Seaman, K. Baugh, K. Cole, E. Stevens, and S. Miller, "Utilization of the Suomi National Polar-Orbiting Partnership (NPP) Visible Infrared Imaging Radiometer Suite (VIIRS) Day/Night Band for Arctic Ship Tracking and Fisheries Management," *Remote Sensing,* vol. 7, pp. 971-989, 2015.

[13] T. N. Polivka, J. Wang, L. T. Ellison, E. J. Hyer, and C. M. Ichoku, "Improving nocturnal fire detection with the VIIRS day–night band," *IEEE Transactions on Geoscience and Remote Sensing,* vol. 54, pp. 5503-5519, 2016.

[14] W. Guo, D. Lu, Y. Wu, and J. Zhang, "Mapping Impervious Surface Distribution with Integration of SNNP VIIRS-DNB and MODIS NDVI Data," *Remote Sensing,* vol. 7, pp. 12459-12477, 2015.

[15] R. C. Sharma, R. Tateishi, K. Hara, S. Gharechelou, and K. Iizuka, "Global mapping of urban built-up areas of year 2014 by combining MODIS multispectral data with VIIRS nighttime light data," *International Journal of Digital Earth,* vol. 9, pp. 1004-1020, 2016.

[16] Y. Dou, Z. Liu, C. He, and H. Yue, "Urban Land Extraction Using VIIRS Nighttime Light Data: An Evaluation of Three Popular Methods," *Remote Sensing,* vol. 9, p. 175, 2017.

[17] B. Yu, M. Tang, Q. Wu, C. Yang, S. Deng, K. Shi, *et al.*, "Urban built-up area extraction from log-transformed NPP-VIIRS nighttime light composite data," *IEEE Geoscience and Remote Sensing Letters,* vol. 15, pp. 1279-1283, 2018.

[18] K. Shi, C. Huang, B. Yu, B. Yin, Y. Huang, and J. Wu, "Evaluation of NPP-VIIRS night-time light composite data for extracting built-up urban areas," *Remote Sensing Letters,* vol. 5, pp. 358-366, 2014.

[19] R. S. Johnson, J. Zhang, E. J. Hyer, S. D. Miller, and J. S. Reid, "Preliminary investigations toward nighttime aerosol optical depth retrievals from the VIIRS Day/Night Band," *Atmospheric Measurement Techniques,* vol. 6, pp. 1245-1255, 2013.

[20] T. M. McHardy, J. Zhang, J. S. Reid, S. D. Miller, E. J. Hyer, and R. E. Kuehn, "An improved method for retrieving nighttime aerosol optical thickness from the VIIRS Day/Night Band," *Atmospheric Measurement Techniques,* vol. 8, pp. 4773-4783, 2015.

[21] R. Li, X. Liu, and X. Li, "Estimation of the PM2.5 Pollution Levels in Beijing Based on Nighttime Light Data from the Defense Meteorological Satellite Program-Operational Linescan System," *Atmosphere,* vol. 6, pp. 607-622, 2015.

[22] Z. Xu, X. Xia, X. Liu, and Z. Qian, "Combining DMSP/OLS Nighttime Light with Echo State Network for Prediction of Daily PM2.5 Average Concentrations in Shanghai, China," *Atmosphere,* vol. 6, pp. 1507-1520, 2015.

[23] J. Wang, C. Aegerter, X. Xu, and J. J. Szykman, "Potential application of VIIRS Day/Night Band for monitoring nighttime surface PM 2.5 air quality from space," *Atmospheric Environment,* vol. 124, pp. 55-63, 2016.

[24] X. Zhao, H. Shi, H. Yu, and P. Yang, "Inversion of Nighttime PM2.5 Mass Concentration in Beijing Based on the VIIRS Day-Night Band," *Atmosphere,* vol. 7, p. 136, 2016.

[25] D. Fu, X. Xia, M. Duan, X. Zhang, X. Li, J. Wang, *et al.*, "Mapping nighttime PM2.5 from VIIRS DNB using a linear mixed-effect model," *Atmospheric Environment,* vol. 178, pp. 214-222, 2018.

[26] X. Li, R. Zhang, C. Huang, and D. Li, "Detecting 2014 Northern Iraq Insurgency using night-time light imagery," *International Journal of Remote Sensing,* vol. 36, pp. 3446-3458, 2015.

[27] X. Li, D. Li, H. Xu, and C. Wu, "Intercalibration between DMSP/OLS and VIIRS night-time light images to evaluate city light dynamics of Syria's major human settlement during Syrian Civil War," *International Journal of Remote Sensing,* vol. 38, pp. 5934-5951, 2017.

[28] M. O. Roman and E. C. Stokes, "Holidays in lights: Tracking cultural patterns in demand for energy services," *Earths Future,* vol. 3, pp. 182-205, Jun 2015.

[29] C. C. M. Kyba, T. Kuester, A. Sanchez de Miguel, K. Baugh, A. Jechow, F. Holker, *et al.*, "Artificially lit surface of Earth at night increasing in radiance and extent," *Sci Adv,* vol. 3, p. e1701528, Nov 2017.

[30] P. Han, J. Huang, R. Li, L. Wang, Y. Hu, J. Wang, *et al.*, "Monitoring Trends in Light Pollution in China Based on Nighttime Satellite Imagery," *Remote Sensing,* vol. 6, pp. 5541-5558, 2014.

[31] J. Ou, X. Liu, X. Li, M. Li, and W. Li, "Evaluation of NPP-VIIRS Nighttime Light Data for Mapping Global Fossil Fuel Combustion CO2 Emissions: A Comparison with DMSP-OLS Nighttime Light Data," *PLoS One,* vol. 10, p. e0138310, 2015.

[32] T. Oda, T. Lauvaux, D. Lu, P. Rao, N. L. Miles, S. J. Richardson, *et al.*, "On the impact of granularity of space-based urban CO2 emissions in urban atmospheric inversions: A case study for Indianapolis, IN," 2017.

[33] C. D. Elvidge, K. Baugh, M. Zhizhin, F. C. Hsu, and T. Ghosh, "VIIRS night-time lights," *International Journal of Remote Sensing,* vol. 38, pp. 5860-5879, 2017.

[34] R. J. Charlson, S. E. Schwartz, J. M. Hales, R. D. Cess, J. J. A. Coakley, J. E. Hansen, *et al.*, "Climate forcing by anthropogenic aerosols," *Science,* vol. 255, pp. 423-430, 1992.

[35] M. Z. Jacobson, "Strong radiative heating due to the mixing state of black carbon in atmospheric aerosols," *Nature,* vol. 409, pp. 695 -697, 2001.

[36] G. de Leeuw, L. Sogacheva, E. Rodriguez, K. Kourtidis, A. K. Georgoulias, G. Alexandri, *et al.*, "Two decades of satellite observations of AOD over mainland China using ATSR-2, AATSR and MODIS/Terra: data set evaluation and large-scale patterns," *Atmospheric Chemistry and Physics,* vol. 18, pp. 1573-1592, 2018.

[37] M. O. Román, Z. Wang, Q. Sun, V. Kalb, S. D. Miller, A. Molthan, *et al.*, "NASA's Black Marble nighttime lights product suite," *Remote Sensing of Environment,* vol. 210, pp. 113-143, 2018.

[38] R. J. Huang, Y. Zhang, C. Bozzetti, K. F. Ho, J. J. Cao, Y. Han, *et al.*, "High secondary aerosol contribution to particulate pollution during haze events in China," *Nature,* vol. 514, pp. 218-22, Oct 9 2014.

[39] J. Wang, B. Zhao, S. Wang, F. Yang, J. Xing, L. Morawska, *et al.*, "Particulate matter pollution over China and the effects of control policies," *Sci Total Environ,* vol. 584-585, pp. 426-447, Apr 15 2017.

[40] B. Silver, C. L. Reddington, S. R. Arnold, and D. V. Spracklen, "Substantial changes in air pollution across China during 2015–2017," *Environmental Research Letters,* vol. 13, p. 114012, 2018.

[41] J. Zhang, J. S. Reid, R. Alfaro-Contreras, and P. Xian, "Has China been exporting less particulate air pollution over the past decade?," *Geophysical Research Letters,* vol. 44, pp. 2941-2948, 2017.

[42] C. Song, L. Wu, Y. Xie, J. He, X. Chen, T. Wang, *et al.*, "Air pollution in China: Status and spatiotemporal variations," *Environ Pollut,* vol. 227, pp. 334-347, Aug 2017.

[43] Y. Wu, S. Zhang, J. Hao, H. Liu, X. Wu, J. Hu, *et al.*, "On-road vehicle emissions and their control in China: A review and outlook," *Sci Total Environ,* vol. 574, pp. 332-349, Jan 1 2017.

[44] K. Baugh, F.-C. Hsu, C. D. Elvidge, and M. Zhizhin, "Nighttime Lights Compositing Using the VIIRS Day-Night Band: Preliminary Results," *Proceedings of the Asia-Pacific Advanced Network,* vol. 35, p. 70, 2013.

[45] N. Baker and H. Kilcoyne, "Joint Polar Satellite System (JPSS) VIIRS radiometric calibration algorithm theoretical basis document (ATBD)," *Goddard Space Flight Center: Greenbelt, MA, USA,* 2013.

[46] B. N. Holben, D. Tanre, A. Smirnov, T. F. Eck, I. Slutsker, N. Abuhassan, *et al.*, "An emerging ground-based aerosol climatology: Aerosol optical depth from AERONET," *Journal of Geophysical Research: Atmospheres,* vol. 106, pp. 12067-12097, 2001.

[47] D. M. Giles, A. Sinyuk, M. G. Sorokin, J. S. Schafer, A. Smirnov, I. Slutsker, *et al.*, "Advancements in the Aerosol Robotic Network (AERONET) Version 3 database–automated near-real-time quality control algorithm with improved cloud screening for Sun photometer aerosol optical depth (AOD) measurements," *Atmospheric Measurement Techniques,* vol. 12, pp. 169-209, 2019.

[48] K. Bessho, K. Date, M. Hayashi, A. Ikeda, T. Imai, H. Inoue, *et al.*, "An Introduction to Himawari-8/9–New-Generation Geostationary Meteorological Satellites," *Journal of the Meteorological Society of Japan. Ser. II,* vol. 94, pp. 151-183, 2016.

[49] G. Dobler, M. Ghandehari, S. E. Koonin, R. Nazari, A. Patrinos, M. S. Sharma, *et al.*, "Dynamics of the urban lightscape," *Information Systems,* vol. 54, pp. 115-126, 2015.

[50] P. Gong, H. Liu, M. Zhang, C. Li, J. Wang, H. Huang, *et al.*, "Stable classification with limited sample: transferring a 30-m resolution sample set collected in 2015 to mapping 10-m resolution global land cover in 2017," *Science Bulletin,* vol. 64, pp. 370-373, 2019.

[51] X. Li, R. Ma, Q. Zhang, D. Li, S. Liu, T. He, *et al.*, "Anisotropic characteristic of artificial light at night – Systematic investigation with VIIRS DNB multi-temporal observations," *Remote Sensing of Environment,* vol. 233, p. 111357, 2019.

[52] Z. Zhang, W. Wu, M. Fan, M. Tao, J. Wei, J. Jin, *et al.*, "Validation of Himawari-8 aerosol optical depth retrievals over China," *Atmospheric Environment,* vol. 199, pp. 32-44, 2019.

[53] X. Cao, Y. Hu, X. Zhu, F. Shi, L. Zhuo, and J. Chen, "A simple self-adjusting model for correcting the blooming effects in DMSP-OLS nighttime light images," *Remote Sensing of Environment,* vol. 224, pp. 401-411, 2019.

[54] J. Zhang, J. S. Reid, S. D. Miller, and F. J. Turk, "Strategy for studying nocturnal aerosol optical depth using artificial lights," *International Journal of Remote Sensing,* vol. 29, pp. 4599-4613, 2008.

[55] Y. L. Zhang and F. Cao, "Fine particulate matter (PM 2.5) in China at a city level," *Sci Rep,* vol. 5, p. 14884, Oct 15 2015.

[56] N. Levin, "The impact of seasonal changes on observed nighttime brightness from 2014 to 2015 monthly VIIRS DNB composites," *Remote Sensing of Environment,* vol. 193, pp. 150-164, 2017.

[57] J. W. Marquis, A. S. Bogdanoff, J. R. Campbell, J. A. Cummings, D. L. Westphal, N. J. Smith, *et al.*, "Estimating Infrared Radiometric Satellite Sea Surface Temperature Retrieval Cold Biases in the Tropics due to Unscreened Optically Thin Cirrus Clouds," *Journal of Atmospheric and Oceanic Technology,* vol. 34, pp. 355-373, 2017.

[58] D. M. Winker, M. A. Vaughan, A. Omar, Y. Hu, K. A. Powell, Z. Liu, *et al.*, "Overview of the CALIPSO Mission and CALIOP Data Processing Algorithms," *Journal of Atmospheric and Oceanic Technology,* vol. 26, pp. 2310-2323, 2009.

[59] Á. Barreto, E. Cuevas, M.-J. Granados-Muñoz, L. Alados-Arboledas, P. M. Romero, J. Gröbner, *et al.*, "The new sun-sky-lunar Cimel CE318-T multiband photometer–a comprehensive performance evaluation," *Atmospheric Measurement Techniques,* vol. 9, pp. 631-654, 2016.

Xuejun Wang received the B.E. degree from the University of Electronic Science and Technology of China, Chengdu, China, in 2016.

She is currently working toward the Ph.D. degree at the Beijing Normal University. Her current research interests include retrieval of atmospheric parameters from satellite data and application of nighttime light satellite data.

Xihan Mu received the B.S. degree in computer science and technology from the College of Information Science and Technology, Beijing Normal University, Beijing, China, in 1999 and the Ph.D. degree in remote sensing from the School of Geography, Beijing Normal University, in 2009. He was a visiting student with the Laboratoire des Sciences de l'Images, de l'Informatique et de la Télédétection, Louis Pasteur University, in 2007 and a visiting scientist with the Commonwealth Scientific and Industrial Research Organisation (CSIRO) in 2016. He is currently with the State Key Laboratory of Remote Sensing Science, Institute of Remote Sensing Science and Engineering, Faculty of Geographical Science, Beijing Normal University, Beijing.

His research interests focus on multiangular remote sensing, particularly in the retrieval/measurement of vegetation structual parameters.

Guangjian Yan received the Ph.D. degree from the Institute of Remote Sensing Applications, Chinese Academy of Sciences, Beijing, China, in 1999. He is currently a Professor with the State Key Laboratory of Remote Sensing Science, Institute of Remote Sensing Science and Engineering, Faculty of Geographical Science, Beijing Normal University, Beijing.

He has published more than 160 papers. His main research interests are multi-angular remote sensing, vegetation remote sensing, radiation budget, scale effect, and scale correction of remote sensing.